Our results imply that the correlations between the atoms in a spin-squeezed Bose-Einstein condensate are strong enough to violate a Bell inequality. This Bell inequality could be violated directly by first localizing the atoms—e.g., through a nondestructive, spin-independent measurement of their position—and then measuring their internal states individually [see section 4 of (*24*)]. Further study of these states may enable insights into many-body correlations outside of the quantum formalism. Our results naturally raise the question of how our witness can be extended to detect genuine multipartite nonlocality (*11*) or to quantify the degree of nonlocality (*29*, *30*), in a similar way as the degree of entanglement can be quantified in terms of k-producibility (Fig. 2) (*20*). Finally, Bell correlations are a resource in quantum information theory—e.g., for certifiable randomness generation. Although Bell-correlation–based randomness has been extracted from two-qubit systems (*31*), an implementation in a many-body system would considerably increase the amount of randomness per experimental run.

REFERENCES AND NOTES

1. N. Brunner, D. Cavalcanti, S. Pironio, V. Scarani, S. Wehner, *Rev. Mod. Phys.* **86**, 419–478 (2014).
2. J. S. Bell, *Between Science and Technology*, A. Sarlemijn, P. Kroes, Eds. (Elsevier, 1990), chap. 6.
3. V. Scarani, *Acta Physica Slovaca* **62**, 347–409 (2012).
4. B. P. Lanyon *et al.*, *Phys. Rev. Lett.* **112**, 100403 (2014).
5. M. Eibl *et al.*, *Phys. Rev. Lett.* **90**, 200403 (2003).
6. Z. Zhao *et al.*, *Phys. Rev. Lett.* **91**, 180401 (2003).
7. J. Hofmann *et al.*, *Science* **337**, 72–75 (2012).
8. W. Pfaff *et al.*, *Nat. Phys.* **9**, 29–33 (2013).
9. M. Ansmann *et al.*, *Nature* **461**, 504–506 (2009).
10. P. D. Drummond, *Phys. Rev. Lett.* **50**, 1407–1410 (1983).
11. G. Svetlichny, *Phys. Rev. D Part. Fields* **35**, 3066–3069 (1987).
12. M. Żukowski, Č. Brukner, *Phys. Rev. Lett.* **88**, 210401 (2002).
13. L. Amico, R. Fazio, A. Osterloh, V. Vedral, *Rev. Mod. Phys.* **80**, 517–576 (2008).
14. I. Bloch, J. Dalibard, W. Zwerger, *Rev. Mod. Phys.* **80**, 885–964 (2008).
15. C. Gross, T. Zibold, E. Nicklas, J. Estève, M. K. Oberthaler, *Nature* **464**, 1165–1169 (2010).
16. I. D. Leroux, M. H. Schleier-Smith, V. Vuletić, *Phys. Rev. Lett.* **104**, 250801 (2010).
17. A. Louchet-Chauvet *et al.*, *New J. Phys.* **12**, 065032 (2010).
18. C. F. Ockeloen, R. Schmied, M. F. Riedel, P. Treutlein, *Phys. Rev. Lett.* **111**, 143001 (2013).
19. A. Sørensen, L.-M. Duan, J. I. Cirac, P. Zoller, *Nature* **409**, 63–66 (2001).
20. A. S. Sørensen, K. Mølmer, *Phys. Rev. Lett.* **86**, 4431–4434 (2001).
21. M. F. Riedel *et al.*, *Nature* **464**, 1170–1173 (2010).
22. P. Hyllus, L. Pezzé, A. Smerzi, G. Tóth, *Phys. Rev. A* **86**, 012337 (2012).
23. J. Tura *et al.*, *Science* **344**, 1256–1258 (2014).
24. Materials and methods are available as supplementary materials on *Science* Online.
25. J.-D. Bancal, N. Gisin, Y.-C. Liang, S. Pironio, *Phys. Rev. Lett.* **106**, 250404 (2011).
26. P. Böhi *et al.*, *Nat. Phys.* **5**, 592–597 (2009).
27. M. Kitagawa, M. Ueda, *Phys. Rev. A* **47**, 5138–5143 (1993).
28. D. J. Wineland, J. J. Bollinger, W. M. Itano, D. J. Heinzen, *Phys. Rev. A* **50**, 67–88 (1994).
29. J.-D. Bancal, C. Branciard, N. Gisin, S. Pironio, *Phys. Rev. Lett.* **103**, 090503 (2009).
30. F. J. Curchod, N. Gisin, Y.-C. Liang, *Phys. Rev. A* **91**, 012121 (2015).
31. S. Pironio *et al.*, *Nature* **464**, 1021–1024 (2010).
32. R. Schmied, P. Treutlein, *New J. Phys.* **13**, 065019 (2011).

ACKNOWLEDGMENTS

We thank R. Augusiak, P. Drummond, and M. Lewenstein for fruitful discussions. R.S., J.-D.B., B.A., M.F., P.T., and N.S. acknowledge support from the Swiss National Science Foundation (SNSF) through grants PP00P2-150579, 20020-149901, and the National Centre of Competence in Research "Quantum Science and Technology" (NCCR QSIT). P.T. acknowledges support from the European Union through the project Simulators and Interfaces with Quantum Systems (SIQS). N.S. acknowledges the Army Research Laboratory Center for Distributed Quantum Information through the project SciNet. J.-D.B. and V.S. acknowledge funding from the Singapore Ministry of Education (partly through Academic Research Fund Tier 3 MOE2012-T3-1-009) and the National Research Foundation of Singapore. Author contributions: N.S. and J.-D.B. initiated the study, with input from R.S. J.-D.B. derived optimal Bell inequalities and performed statistics tests, discussing with R.S., N.S., and V.S. R.S. and P.T. derived the witnesses from the Bell inequality, with support from J.-D.B. and N.S. B.A., M.F., and R.S. performed experiments and analyzed data, supervised by P.T. All authors discussed the results and contributed to the manuscript.

SUPPLEMENTARY MATERIALS

www.sciencemag.org/content/352/6284/441/suppl/DC1
Materials and Methods
Figs. S1 to S4
Reference (*33*)

13 November 2015; accepted 11 March 2016
10.1126/science.aad8665

GEOLOGY

Continental arc volcanism as the principal driver of icehouse-greenhouse variability

N. Ryan McKenzie,[1,2,3]* Brian K. Horton,[2,4] Shannon E. Loomis,[2] Daniel F. Stockli,[2] Noah J. Planavsky,[1] Cin-Ty A. Lee[5]

Variations in continental volcanic arc emissions have the potential to control atmospheric carbon dioxide (CO_2) levels and climate change on multimillion-year time scales. Here we present a compilation of ~120,000 detrital zircon uranium-lead (U-Pb) ages from global sedimentary deposits as a proxy to track the spatial distribution of continental magmatic arc systems from the Cryogenian period to the present. These data demonstrate a direct relationship between global arc activity and major climate shifts: Widespread continental arcs correspond with prominent early Paleozoic and Mesozoic greenhouse climates, whereas reduced continental arc activity corresponds with icehouse climates of the Cryogenian, Late Ordovician, late Paleozoic, and Cenozoic. This persistent coupled behavior provides evidence that continental volcanic outgassing drove long-term shifts in atmospheric CO_2 levels over the past ~720 million years.

Earth experienced multiple shifts in climate state over the past ~720 million years (My), with extensive icehouse intervals during the Cryogenian (*1*, *2*), latest Ordovician (*3*), late Paleozoic (*4*), and mid-late Cenozoic alternating with greenhouse intervals during the early Paleozoic and Mesozoic–early Cenozoic eras (*5*, *6*). These shifts are attributed to changes in the partial pressure of atmospheric carbon dioxide (P_{CO_2}) (*5*–*8*). Long-term (≥10^6 years) changes in P_{CO_2} are controlled by the magnitude of carbon input to the ocean-atmosphere system from volcanic and metamorphic outgassing, as well as the removal of this carbon primarily through silicate weathering and subsequent precipitation and burial of carbonate minerals, along with organic carbon burial (*8*, *9*). Although sporadic processes such as enhanced plume activity (*10*) and mountain building (*11*) have been invoked as drivers of specific greenhouse or icehouse intervals, no unifying model explains all of the observed fluctuations.

Arc magmatism along continental-margin subduction zones is thought to contribute more CO_2 to the atmosphere than other volcanic systems, owing to decarbonation of carbonates stored in the continental crust of the upper plate (*12*–*16*). Although direct measurements of CO_2 outgassing rates are limited, current continental volcanic arc (CVA) emissions are estimated to be as

[1]Department of Geology and Geophysics, Yale University, New Haven, CT 06511, USA. [2]Department of Geological Sciences, Jackson School of Geosciences, University of Texas at Austin, Austin, TX 78712, USA. [3]Department of Earth Sciences, University of Hong Kong, Pokfulam, Hong Kong, China. [4]Institute for Geophysics, Jackson School of Geosciences, University of Texas at Austin, Austin, TX 78712, USA. [5]Department of Earth Sciences, Rice University, Houston, TX 77005, USA.
*Corresponding author Email: ryan.mckenzie@yale.edu

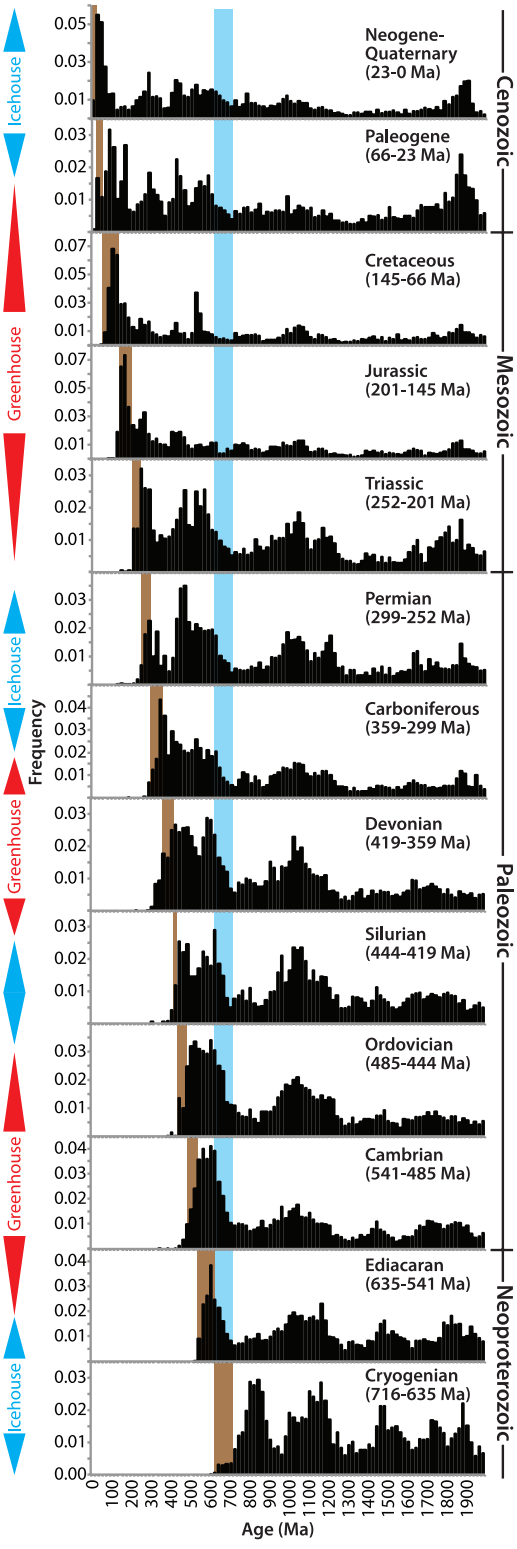

Fig. 1. Normalized composite zircon U-Pb age distributions for global Cryogenian to modern sedimentary deposits. Data are arranged by geologic period and plotted in age histograms using 20-My bins. Vertical brown bars demarcate the depositional age range of each geologic period. Vertical blue bars highlight the Cryogenian glacial interval to note the persistent low abundance of zircons transitioning into this interval.

high as ~150 teragrams C per year (Tg/year), in contrast to 12 to 60 Tg/year from ocean ridges and 1 to 30 Tg/year from oceanic intraplate volcanoes (*14*). Therefore, the spatial distribution of CVAs through geologic time, which varies due to changes in plate tectonic regimes (*17*), may play a prominent role in regulating Earth's climate state.

Because variations in CVA activity have few constraints through Earth history, it is difficult to model their role as drivers of climate change (*16*). Burial, erosion, or destruction of the arc can hinder our ability to track CVA systems in deep geologic time. The sedimentary record, however, provides an effective means to track the past presence of CVA systems. Although original arc rocks may be gone, their eroded components are distributed and archived in many adjacent sedimentary basins. Zircon, a key mineral for U-Pb geochronology, is chemically and physically resistant to degradation. Zircon grains are capable of enduring the rigors of erosion, transport, reworking, burial, moderate to high degrees of metamorphism, subduction, and return to the surface through magmatic processes, thus yielding particularly long residence times in the continental crust (*18*). Whereas mantle-derived mafic rocks (from high-temperature, low-silica dry magmas) associated with continental rifts, spreading ridges, and flood basalts have low-zircon yields, zircon-fertile rocks are mostly produced by low-temperature, high-silica hydrous melts along continental subduction zones (*19*). Siliciclastic strata deposited near active CVAs contain abundant young zircon grains (i.e., zircons with U-Pb crystallization ages close to the stratal depositional age) defining distinct age populations that track regional magmatic arc flare-ups (*20*), whereas large igneous provinces (LIPs), rift systems, and passive margins generally lack substantial young zircon populations (*21*, *22*). Oceanic island arcs do not affect the continental sedimentary record until accretion, which introduces older grains. Therefore, we can employ the relative abundance of young detrital zircon grains in the stratigraphic record to assess the regional presence and importance of CVA systems.

We compiled ~120,000 new and published single-grain detrital zircon U-Pb ages from globally distributed clastic sedimentary rocks to track the spatial distribution of CVAs from the Cryogenian to the present. Using U-Pb data from strata with depositional ages constrained to at least the geologic period, we generated global age distributions to evaluate relative shifts in the abundance of young zircon grains, which are linked to regional silicic magmatism. Because global sampling is incomplete and the quantity of age data available from different regions is variable, we applied a normalization process for our composite distributions (*23*). First, U-Pb ages were arranged regionally by geographic location (26 zones) (fig. S1) and temporally by geologic period (13 intervals) (table S1). Age frequency distributions were established for all data, and then the individual regional distributions were equally weighted to create global composite distributions for each geologic period. For periods lacking data in prominent regions with reasonably known geologic histories, we used regional age data from the next youngest period to backfill the empty bin (*23*). An outlier test was performed to identify anomalous data sets that significantly skewed the composite distributions and to ensure that the signal was indeed global (*23*).

We found that composite age distributions from rocks deposited during icehouse intervals contain relatively low proportions of young zircon, whereas distributions from greenhouse intervals are skewed toward younger populations (Fig. 1). This is best illustrated by the cumulative age distributions in which the Cryogenian, Silurian, Permian, and Cenozoic icehouse intervals yield low proportions of young zircon grains but the Cambrian, Jurassic, and Cretaceous greenhouse periods yield the greatest proportions of young grains (Figs. 2 and 3). The mean ages of the young populations in each interval vary with respect to modeled Phanerozoic CO_2 value, as the young mean ages converge on the depositional age transitioning into greenhouse climates and deviate from the depositional age during icehouse climates (Fig. 3). Overall, these data demonstrate a direct link between shifts in global detrital zircon production, CVA distribution, and major climate transitions over the past ~720 My.

The relationships between icehouse-greenhouse transitions and CVA spatiotemporal variations fit within the paleogeographic framework of continents. Continental breakup requires the opening of new ocean basins and the generation of new oceanic lithosphere. This, in turn, requires the consumption of old oceanic lithosphere elsewhere along subduction zones and produces CVAs, whereas continental collisions shut down subduction and lessen the global length of CVAs (*15*, *17*, *22*, *24*). Therefore, intervals following continental breakup will consist of high continent dispersal with spatially extensive CVAs, and intervals during and after continental collision will consist of reduced CVAs.

The extent of the low-latitude Cryogenian Sturtian [716 million years ago (Ma)] and Marinoan (635 Ma) glaciations requires anomalously low levels of atmospheric CO_2 (*25*, *26*). Increased silicate weathering due to continental rifting and emplacement of the low-latitude Franklin LIP, which produced highly weatherable mafic rocks, are cited as primary mechanisms for CO_2 consumption to trigger these "snowball Earth" events (*2*, *27*). However, Mesoproterozoic (~1400 Ma) emplacement of prominent low-latitude LIPs did

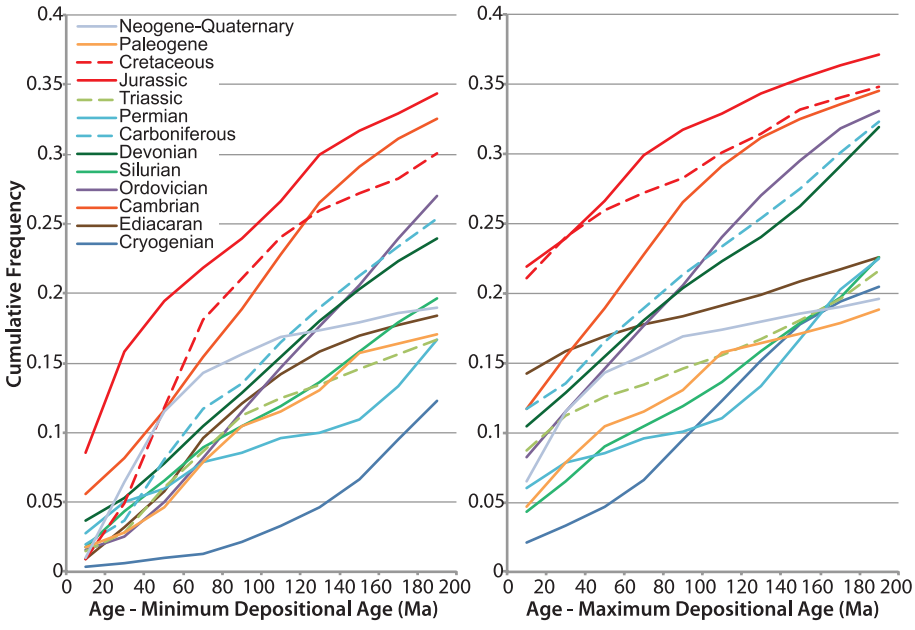

Fig. 2. Cumulative distribution functions (CDFs) of young zircon U-Pb ages. CDFs for each geologic period (greenhouse, warm colors; icehouse, cool colors) relative to the approximate minimum (left) and maximum (right) depositional ages. CDFs were normalized to zero by subtracting the ages from periods younger than the minimum and maximum depositional ages, respectively (*23*). Consideration of the young grain abundance relative to maximum depositional age removes inherent biases related to the differential duration of geologic periods relative to sample depositional ages. A 200-My window represents a reasonable approximation of the typical duration of CVA activity.

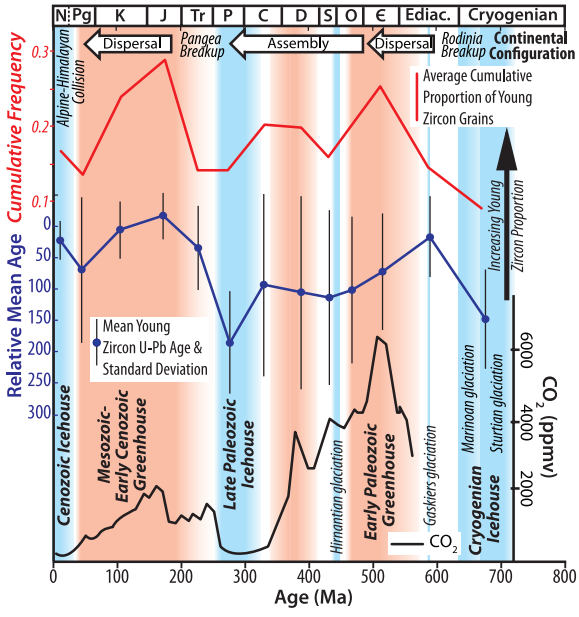

Fig. 3. Cumulative proportion of young grains compared to the mean age of young grains, configuration of continents, icehouse-greenhouse intervals, and modeled Phanerozoic CO_2 levels. Average cumulative proportion of young ages within 200 My of minimum depositional ages (from Fig. 2) (red line), and mean young ages calculated from the 300-My window relative to the minimum depositional age used in our statistical analysis (*23*) (blue line), are plotted against the average depositional age of each period. A value of 0 is assigned where the mean young age equals the average depositional age. Comparison of the cumulative proportion to the mean young ages provides insight into the relative abundance of young to older arc-derived grains (e.g., both the Ediacaran and Triassic periods contain low abundances of young to old grains coupled with relatively young mean ages, indicating that most young grains are from young CVAs). The low proportions of young grains and relatively older mean ages in the Cryogenian and Permian indicate that older grains dominate the distributions. The CO_2 curve was taken from (*7*). ppmv, parts per million by volume. N, Neogene; Pg, Paleogene; K, Cretaceous; J, Jurassic; Tr, Triassic; P, Permian; C, Carboniferous; D, Devonian; S, Silurian; O, Ordovician; Є, Cambrian; Ediac., Ediacaran.

not yield known glaciations (*28*). The Phanerozoic record is also replete with LIPs (*29*) that did not induce glaciations. The Siberian traps erupted at the end of the late Paleozoic icehouse interval without subsequent glaciation, albeit in a high-latitude paleogeographic position. The Khalkarindji, Central Atlantic, and Deccan provinces formed at lower latitudes (*30*), and contrastingly, these events all correspond with greenhouse intervals. Although the Franklin LIP was broadly contemporaneous with the Sturtian, there is no LIP matching the Marinoan glaciation. We find the assumption of a primary relationship between LIP emplacement and Cryogenian glaciations difficult to justify. Rather, we postulate that Cryogenian glaciations resulted from a major drop in volcanic CO_2 fluxes associated with the assembly of Rodinia.

The Rodinia supercontinent formed by ~900 Ma and underwent protracted Neoproterozoic rifting starting as early as 750 Ma, with diachronous final breakup around 600 Ma (*31*, *32*). Rodinia's long existence included an interval of reduced CVAs with a progressive increase throughout the period of Neoproterozoic breakup, as evidenced by a young zircon lull ~720 Ma at the transition to the Cryogenian glacial interval and an increase toward the end of the interval (Fig. 1). The influence of diminished volcanic CO_2 fluxes on Cryogenian glaciations has been suggested (*22*), but our expanded data set illustrates the pronounced scale of this reduction, with the Cryogenian yielding the lowest proportion of young grains of all subsequent geologic periods (Figs. 1, 2, and 3). Nearly all regions contain data from Marinoan glacial deposits (~635 Ma) roughly equal to the minimum depositional age of the Cryogenian period, which makes for a pronounced gap between the minimum depositional age and the youngest abundant zircon population. The low-latitude Paleoproterozoic Huronian glaciations (2400 to 2300 Ma), the last known glaciations before the Cryogenian, also coincide with a prominent magmatic gap (*33*). Therefore, we assert that the severity of Cryogenian glaciations and the prominence of the zircon age lull are not coincidences and that the major reduction in the volcanic CO_2 flux was critical to allow extensive low-latitude glaciations.

A broad dispersal of continents persisted during the Ediacaran and Cambrian periods, until the assembly of Gondwana was complete by the Middle Ordovician (*22*). The Cambrian, which had the highest P_{CO_2} of the Phanerozoic (*5*–*7*) (Fig. 3), was followed by Ordovician cooling that culminated with the Hirnantian glaciations (~445 Ma) (*3*). Ediacaran deposits show a notable increase in both the abundance and mean age of young grains, and Cambrian deposits contain high proportions of young zircon (Figs. 1, 2, and 3). Ordovician deposits show a reduction in young grains, and Silurian deposits, which account for the ~20-My interval following the Hirnantian glaciation, contain low proportions of young zircon (Figs. 2 and 3). Continental coalescence continued through the Paleozoic by newly formed subduction zones until the final amalgamation of Pangea by

the Carboniferous-Permian transition (*24*). Mid-Paleozoic warm conditions were followed by the late Paleozoic icehouse, which spanned at least from the Late Carboniferous to the Early Permian (*4*). The proportions of young zircon grains are modest in Devonian-Carboniferous strata and low in Permian strata. Pangea rifting initiated by the Triassic, with complete breakup by Jurassic-Cretaceous time marking another interval of relatively high continent dispersal, until Paleogene Alpine-Himalayan collision along southern Eurasia closed the Tethys Ocean, substantially reducing global CVA length (*15*, *34*). Triassic deposits show an increase in young zircon grains, with very high proportions in the Jurassic-Cretaceous greenhouse world (*6*). A reduction in young zircon populations for Paleogene and Neogene-Quaternary deposits matches the Cenozoic record of global cooling (*35*). In sum, the abundance of young zircon grains in Cambrian and Jurassic-Cretaceous strata reflects high CVA distributions during those intervals of high continent dispersal and greenhouse climates, whereas the low abundance during the Cryogenian, Silurian, Permian, and Cenozoic demonstrates diminished CVA distributions during those intervals of continent amalgamation and icehouse climates.

Phanerozoic GEOCARB CO_2 models (*7*) (Fig. 3) broadly correspond with the CVA record because these models use approximated seafloor-spreading rates, largely inferred from Phanerozoic sea-level records, to estimate volcanic CO_2 fluxes. Spreading rates are driven by slab pull and suction associated with subduction, which increases with slab length (*36*). Geodynamic models demonstrate that spreading rates and sea level increase during intervals of continent dispersal (*37*). The composite U-Pb age distributions are normalized regionally, and the relative shifts in young zircon abundance are dependent on global shifts rather than accelerated production in a particular region. Therefore, the age distributions represent global zircon production and track the spatial distributions of CVAs through time. Increased fluxes from spreading centers due to rapid subduction during intervals of continent dispersal would certainly contribute to overall CO_2 outgassing, but the flux potential from CVAs is far greater (*12*, *14*, *15*).

A lack of constraints on deep-time volcanic CO_2 emissions has prompted many studies to propose changes in silicate weathering as the primary control on P_{CO_2} variations (*9*, *38*). This notion appears to be at odds with the geologic record. No consistent relationship exists between LIP emplacement, which could change the weatherability of the crust, and long-term climate. Temporal variations in global uplift also cannot explain intervals of climate change. Noncollisional convergent margins with CVAs can produce large mountain belts through arc magmatism and retroarc shortening that thicken the crust of the upper plate. The extensive North and South American Cordilleras along the eastern Pacific subduction zones are prime examples. The two highest mountain belts on Earth, the Andes and the Himalaya, formed under similar contractional tectonic regimes, despite their contrasting settings along subduction and collisional margins. Although increased weathering and erosion may be expected during intervals of extensive CVA dispersion due to a combination of uplift, production of weatherable volcanics, and moisture availability from adjacent oceans, intervals of continent dispersal correspond with greenhouse climates. Similarly, continental assembly should generally insulate continent collision belts from oceans and reduce weathering rates, yet these intervals correspond with icehouse climates. The paleogeographic position of continents can influence local weathering rates, but Cryogenian glaciations occurred with continents concentrated at low latitudes (*32*), whereas large landmasses were at high latitudes during late Paleozoic icehouse conditions (*30*). Likewise, the transition from the early Paleozoic greenhouse to the Hirnantian icehouse occurred without drastic changes in paleogeography. Therefore, we find no causative links between continental paleogeography or topographic variation and global climate change.

Silicate weathering increases with increased temperature, providing a feedback that prevents runaway greenhouse conditions and is critical to maintaining a habitable environment for life (*9*, *38*). The temperature control on silicate weathering means that it operates as a function of, and is largely dependent on, the CO_2 flux into the atmosphere (*39*). Therefore, the input flux should exert the first-order control on atmospheric CO_2 fluctuations that dictate baseline climate. Spatiotemporal variation in the distribution of CVAs—contributors of the largest and most variable CO_2 input flux—exhibits a consistent correlation with all major icehouse-greenhouse transitions over the past ~720 My. Further, the correspondence of a prominent magmatic lull with the extensive Paleoproterozoic Huronian glaciations suggests that CVA CO_2 outgassing was a principal driver of Earth's long-term climate variability for the past ~2.4 billion years.

REFERENCES AND NOTES

1. P. F. Hoffman, A. J. Kaufman, G. P. Halverson, D. P. Schrag, *Science* **281**, 1342–1346 (1998).
2. F. A. Macdonald *et al.*, *Science* **327**, 1241–1243 (2010).
3. S. Finnegan *et al.*, *Science* **331**, 903–906 (2011).
4. I. P. Montañez, C. J. Poulsen, *Annu. Rev. Earth Planet. Sci.* **41**, 629–656 (2013).
5. N. M. Bergman, T. M. Lenton, A. J. Watson, *Am. J. Sci.* **304**, 397–437 (2004).
6. D. L. Royer, R. A. Berner, I. P. Montanez, N. J. Tabor, D. J. Beerling, *GSA Today* **14**, 4–10 (2004).
7. R. A. Berner, Z. Kothavala, *Am. J. Sci.* **301**, 182–204 (2001).
8. R. A. Berner, A. C. Lasaga, R. M. Garrels, *Am. J. Sci.* **283**, 641–683 (1983).
9. L. R. Kump, S. L. Brantley, M. A. Arthur, *Annu. Rev. Earth Planet. Sci.* **28**, 611–667 (2000).
10. R. L. Larson, *Geology* **19**, 547–550 (1991).
11. M. E. Raymo, W. F. Ruddiman, *Nature* **359**, 117–122 (1992).
12. M. R. Burton, G. M. Sawyer, D. Granieri, *Rev. Mineral. Geochem.* **75**, 323–354 (2013).
13. R. Dasgupta, *Rev. Mineral. Geochem.* **75**, 183–229 (2013).
14. C.-T. A. Lee, J. S. Lackey, *Elements* **11**, 125–130 (2015).
15. C.-T. A. Lee *et al.*, *Geosphere* **9**, 21–36 (2013).
16. D. M. Kerrick, K. Caldeira, *Chem. Geol.* **145**, 213–232 (1998).
17. P. G. Silver, M. D. Behn, *Science* **319**, 85–88 (2008).
18. G. Gehrels, *Annu. Rev. Earth Planet. Sci.* **42**, 127–149 (2014).
19. C.-T. A. Lee, O. Bachmann, *Earth Planet. Sci. Lett.* **393**, 266–274 (2014).
20. S. R. Paterson, M. N. Ducea, *Elements* **11**, 91–98 (2015).
21. P. A. Cawood, C. J. Hawkesworth, B. Dhuime, *Geology* **40**, 875–878 (2012).
22. N. R. McKenzie, N. C. Hughes, B. C. Gill, P. M. Myrow, *Geology* **42**, 127–130 (2014).
23. Materials and methods are available as supplementary materials on *Science* Online.
24. D. C. Bradley, *Earth Sci. Rev.* **108**, 16–33 (2011).
25. R. T. Pierrehumbert, D. S. Abbot, A. Voigt, D. Koll, *Annu. Rev. Earth Planet. Sci.* **39**, 417–460 (2011).
26. D. P. Schrag, R. A. Berner, P. F. Hoffman, G. P. Halverson, *Geochem. Geophys. Geosyst.* **3**, 1–21 (2002).
27. Y. Donnadieu, Y. Goddéris, G. Ramstein, A. Nédélec, J. Meert, *Nature* **428**, 303–306 (2004).
28. N. J. Planavsky *et al.*, in *Earth-Life Transitions: Paleobiology in the Context of Earth System Evolution*, P. D. Polly, J. J. Head, D. L. Fox, Eds. (The Paleontological Society, 2015), vol. 21, pp. 47–82.
29. R. E. Ernst, K. L. Buchan, I. H. Campbell, *Lithos* **79**, 271–297 (2005).
30. C. R. Scotese, Plate tectonic maps and continental drift animations: PALEOMAP Project (2001); www.scotese.com.
31. D. A. D. Evans, *Geol. Soc. Am. Bull.* **125**, 1735–1751 (2013).
32. Z. X. Li *et al.*, *Precambrian Res.* **160**, 179–210 (2008).
33. K. C. Condie, C. O'Neill, R. C. Aster, *Earth Planet. Sci. Lett.* **282**, 294–298 (2009).
34. D. G. Van Der Meer *et al.*, *Proc. Natl. Acad. Sci. U.S.A.* **111**, 4380–4385 (2014).
35. J. Zachos, M. Pagani, L. Sloan, E. Thomas, K. Billups, *Science* **292**, 686–693 (2001).
36. C. P. Conrad, C. Lithgow-Bertelloni, *J. Geophys. Res.* **109**, B10407 (2004).
37. A. Lenardic *et al.*, *Geochem. Geophys. Geosyst.* **12**, Q10016 (2011).
38. Y. Goddéris, Y. Donnadieu, G. Le Hir, V. Lefebvre, E. Nardin, *Earth Sci. Rev.* **128**, 122–138 (2014).
39. R. A. Berner, K. Caldeira, *Geology* **25**, 955–956 (1997).

ACKNOWLEDGMENTS

N.R.M and B.K.H. acknowledge funding from NSF-Tectonics grant EAR-1348031. N.R.M. and S.E.L. acknowledge the Jackson School of Geosciences Distinguished Postdoctoral Program, University of Texas at Austin. N.R.M. acknowledges the Flint Postdoctoral Program, Yale University. C.-T.A.L. acknowledges funding from NSF award OCE-1338842. We thank C. Reinhard, M. Brandon, D. Evans, A. Smye, and O. Anfinson for helpful discussions. This is University of Texas Institute for Geophysics contribution no. 2955. Literature sources and data tables for new U-Pb ages used in the compilation are provided in the supplementary materials.

SUPPLEMENTARY MATERIALS

www.sciencemag.org/content/352/6284/444/suppl/DC1
Materials and Methods
Figs. S1 to S4
Tables S1 and S2
References (*40*–*239*)
Data S1

4 October 2015; accepted 11 March 2016
10.1126/science.aad5787

Continental arc volcanism as the principal driver of icehouse-greenhouse variability

N. Ryan McKenzie, Brian K. Horton, Shannon E. Loomis, Daniel F. Stockli, Noah J. Planavsky and Cin-Ty A. Lee (April 21, 2016)

Science **352** (6284), 444-447. [doi: 10.1126/science.aad5787]

Editor's Summary

Erosion overwhelmed by eruption

Volcanism and erosion can feed into long-term climate change, but determining their relative importance is challenging. Erosion is known to be a carbon sink and is thought to play an outsized role in shifting global climate. However, McKenzie *et al.* suggest that long-term oscillations in climate may be tied to the amount of continental arc volcanism (see the Perspective by Kump). A global compilation of arc volcano-produced zircons over the past 700 million years revealed good correlation between warm and cool epochs with the waxing and waning of volcanism. Thus, volcanism may be a more important driver and erosion a less important sink for very long-term climate changes.

Science, this issue p. 444; see also p. 411